A HIGH RESOLUTION FULL EARTH DISK MODEL FOR MICROWAVE OBSERVATIONS FROM GEO

Boon H Lim[1], Christopher S Ruf[1] and Alan B Tanner[2]

1. Atmospheric, Oceanic and Space Sciences Dept.
University of Michigan
Ann Arbor, MI USA 48109-2143
bhlim@umich.edu cruf@umich.edu

2. Jet Propulsion Laboratory
California Institute of Technology
Pasadena, CA USA 91011
alan.b.tanner@jpl.nasa.gov

Abstract – A proposed instrument for deployment on next generation Geostationary Operational Environmental Satellite (GOES) platforms is the Geostationary Synthetic Thinned Aperture Radiometer (GeoSTAR) [1, 2]. A high resolution full earth disk model has been developed to aid in the development of the instrument design and to characterize sensor performance. A variety of publicly available geophysical fields are used as data inputs into a full radiative transfer model that also accounts for the propagation and viewing geometries from GEO. The resulting model simulates full disk microwave images with the highest known resolution. The model can be used in concert with an instrument simulator to conduct design tradeoff studies. With the capability of generating high resolution brightness images at different frequencies, atmospheric profile retrievals can be evaluated.

I. INTRODUCTION

Operating at 50 GHz and 183 GHz, GeoSTAR will provide temperature and water vapor soundings at higher temporal and spatial resolution than are currently available. The design targets a nadir resolution of 50 km (50 GHz) and 25 km (183 GHz) with new images generated approximately hourly. The key parameter in the instrument design space is the minimum tolerable noise of the output images. This one parameter impacts the integration time, antenna gain (and consequently the antenna topology) [3], receiver design and calibration scheme. Ideally, an Observing System Simulation Experiment (OSSE) would determine the impact changes in the hardware design would have on the science. However, currently the resources are not available for a full scale OSSE.

Reduced spatial scale Earth models have been successfully used to examine array distortion errors [4]. While appropriate for antenna redundancy and perturbation analysis, these models do not accurately account for the high spatial components of the visibility measurement[1]. Additional analyses performed comparing GeoSTAR to a traditional scanning radiometer have the desired spatial resolution (~5 km) but focus only on regional areas [5]. To this end a high resolution full disk model is crucial to investigating the instrument performance and design parameters, especially of the high frequency components of the visibility and the impact on retrievals. The initial full earth disk model will be created at 50 GHz to test the temperature sounding channels. Once a database of images is generated, atmospheric profile retrievals can be performed to assess their usability at high incident angles. The resolution of the model is selected to be 10 km to be compatible with the expected spatial resolution of the 183 GHz channels.

II. FULL DISK MODEL ASSUMPTIONS

A. High Frequency Visibility Contributors

The key assumption in the generation of the model is that not all atmospheric parameters vary significantly at the spatial scales of the measurement. In fact, most parameters vary smoothly spatially and hence contribute minimally to the high frequency components of visibility. The major contributors to the high frequency visibilities are sharp transitions, in particular:-

1. Earth disk / Cosmic Background
2. Coastlines
3. Clouds

Of these three, only the clouds change on the time scales of the measurement. The other two parameters vary minimally with seasons if at all. These contributors define the parameter

This work was supported by NASA Headquarters under the NASA Earth and Space Science Fellowship Program – Grant NNG05GP47H.

[1] Visibilities can be interpreted simply as the image measured in the spatial Fourier domain, which are what GeoSTAR and other spatial interferometric imager's measure.

resolution requirements. It is this assumption that allows us to combine the appropriate datasets to produce the full resolution inputs into the radiative transfer model.

B. Scattering-free Assumption at 50 GHz

The current model does not include a scattering model for precipitation, liquid or ice. The effects of liquid scattering are known to be minimal at 50 GHz since absorption effects dominate, except for large hydrometeors in stratiform and convective precipitation cells. Moreover, ice scattering aloft, especially in strong convective storm cells, is known to produce brightness temperature darkening and these effects are also unaccounted for in the present model. A scattering model will be integrated when the model is extended for operation at 183 GHz.

III. Geophysical Parameter Datasets

Table 1 summarizes the various geophysical parameter datasets that are used. The National Centers for Environmental Prediction (NCEP) Global Data Assimilation System (GDAS) provides the vertical profiles on which the other parameters are overlaid. Highlighted parameters (the cloud product and land mask) have the highest spatial resolution as required from the assumptions. A total of 6 different datasets from a variety of sources are used to generate the final images.

Table 1: Summary of Geophysical Parameter Datasets

Measured Parameters	Data Source	Spatial Res.	Temporal Res.
Land Emissivity	NWPG France	50km x 50km	Monthly Averages
Ocean Wind Speed	NCEP GDAS	100km x 100km	6 Hour Refresh
Sea Surface Temp.	NCEP GDAS	100km x 100km	6 Hour Refresh
Sea Surface Salinity	WOA 2005	100km x 100km	Monthly Averages
Temperature Profile	NCEP GDAS	100km x 100km	6 Hour Refresh
Geopotential Height	NCEP GDAS	100km x 100km	6 Hour Refresh
Humidity Profile	NCEP GDAS	100km x 100km	6 Hour Refresh
Surface Parameters	NCEP GDAS	100km x 100km	6 Hour Refresh
Cloud Liquid/Ice Water	NASA LaRC	8km x 8km	~3 Hour Refresh
Cloud Top/Bottom Temp.	NASA LaRC	8km x 8km	~3 Hour Refresh
Land Sea Mask	GODAE GHSTT	1km x 1km	Generated in 2002
Digital Elevation Map	NGDC	4km x 4km	Generated in 2006

A. Use of Monthly Averages

Both the land emisivity and sea surface salinity maps are monthly averages, which is sufficient for our use. These products vary primarily with season and are often simply replaced by a constant value in most other analyses. A monthly average adequately models the actual parameter state, especially when combined with GDAS surface temperatures.

B. Land Sea Masks

The resolution of the land-sea mask is reduced to match our needs by taking the aggregate weight of the surrounding pixels for an effective 10 km resolution. In addition, this fractional weight is also used to weight the contributions of the emissivity maps so that the final image appears as it would with the effective 10 km resolution. This processing is preferable, as compared to using simple binary masks, in order to prevent the introduction of artificial high frequency components.

C. Langley Cloud and Radiation Research Group

The cloud product is a new dataset obtained from the Cloud and Radiation Research Group at NASA Langley Research Center. Full disk parameters are available for GOES West, GOES East and METEOSAT, derived from its VIS/IR channels [6]. The product is ideal for our use as it provides a 'snapshot' of the cloud products over the entire area of interest. Previous iterations of the product were only available for regional areas.

IV. Geophysical Parameter Models

In concert with the input geophysical parameter datasets, several additional parameters have to be derived. The models on which these derivations are based are described next.

A. Ocean Emissivity

The dielectric constant of water is computed from the Klein-Swift model [7]. A correction for roughness and foam fraction is calculated using coefficients from FastEM2 developed for RTTOV [8]. The specific coefficients used are those generated for the Advanced Microwave Sounding Unit (AMSU) on board the current Polar-orbiting Operational Environmental Satellite (POES) performing GEOSTAR-like measurements.

B. Gaseous Absorption

Absorption for both atmospheric gases and gaseous water vapor is derived performed using Rosenkranz98 [9].

C. Cloud Parameters

Cloud liquid absorption is calculated using the assumption that absorption is proportional to the column density of the cloud liquid [10]. Cloud liquid profiles are assumed to be constant given a liquid water path. This is valid to first order because no distinction is made between different cloud types in the model. Finally, the vertical profile of liquid in the freezing layer is modeled by an exponential lapse [11].

V. Grids

A. Geophysical Parameter Grid

The geophysical parameter grid is a 10 km equal area grid. Essentially this grid has variable longitude spacing that is dependent on latitude. The longitude spacing increases to compensate for the decreasing circumference of the latitude circle as the location approaches either pole.

B. GeoSTAR Image Grid

The GeoSTAR image grid is equally spaced in the direction cosine domain. The nadir looking pixel size on the earth disk is 10 km, and increases off nadir.

C. Radiative Transfer Calculation

Each GeoSTAR pixel is calculated independently with a slant path determined from the GOES incidence angles. The downwelling and upwelling components are calculated

separately as they differ according to the viewing geometry. A plane parallel atmosphere approximation is used which is valid for all but the largest incident angles. At the larger incidence angles, the atmospheric opacity dominates.

VI. Brightness Temperature (T_B) Images

Figure 1 shows a model output T_B image generated from geophysical datasets for 1200 UTC on 17 March 2008 for the 50.3 GHz channel at vertical polarization (V-Pol). This is effectively what GeoSTAR will image from a GOES East platform, with the exception of the cosmic background radiation which has been removed to improve visual contrast. Surface features can be discerned as this is on the lower wing of the oxygen line where the atmosphere is fairly transparent.

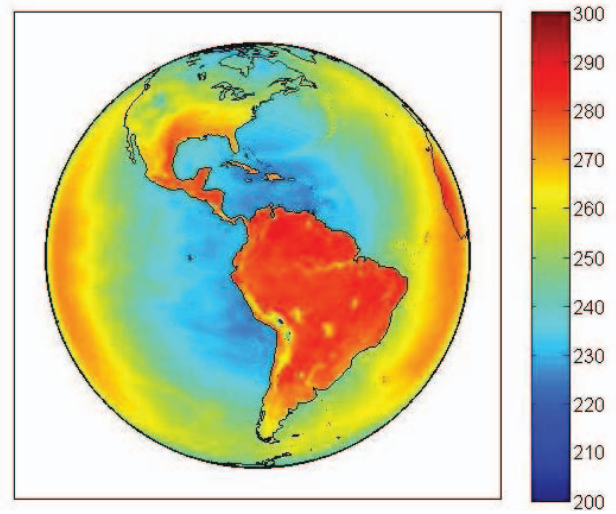

Figure 1: 17 Mar 2008 12z T_B 50.3 GHz V-Pol [K]

The behavior of T_B with incidence angle has been verified independently over both land and ocean by comparison with theoretical results and found to compare favorably.

In Figure 1, several features are noteworthy. Storms in the North and South Atlantic are visible even with the large color scale and increased opacity at larger incident angles. Surface features such as major rivers are also visible, although somewhat 'blurred' by the spatial resolution.

Various atmospheric parameters can be controlled during the generation of the T_B images. Figure 2 shows an example of the difference in T_B at horizontal polarization (H-Pol) due to winds only (wind excess emissivity). H-Pol is selected as it has a larger emissivity response. The inset image shows the input wind map with maximum winds of ~25 m/s.

Figure 3 shows the atmospheric transmissivity at 50.3 GHz with clouds removed. Even at the transparent channel, the earth disk limbs are optically thick. Areas of high altitude (*e.g.* the Rockies and the Andes) exhibit very high transmissivity.

The T_B images given an atmospheric state show excellent quality and high resolution. Combining the images with an instrument model will allow for numerous tradeoff analyses. With images at various frequencies along the wing of the oxygen line, atmospheric profile retrievals can be performed.

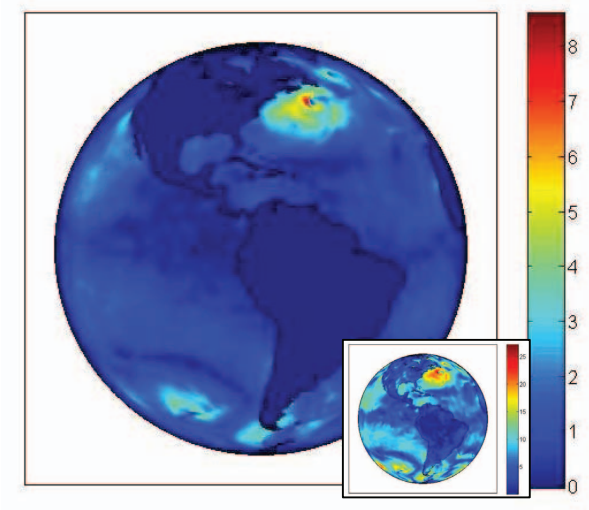

Figure 2: 17 Mar 2008 12z Excess T_B due to winds 50.3 GHz H-Pol [K]

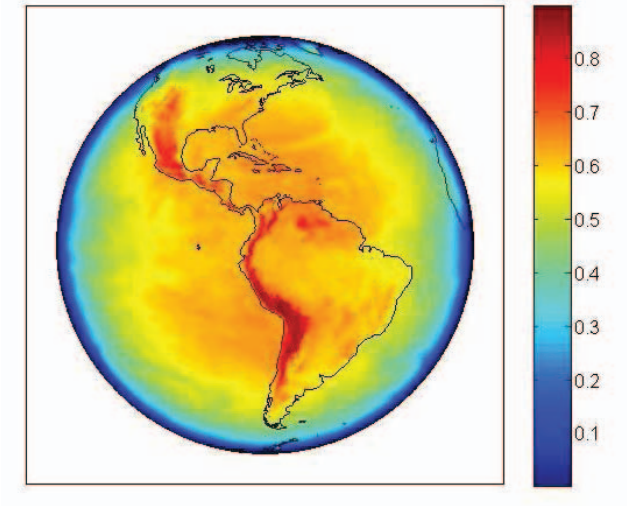

Figure 3: 17 Mar 2008 12z Atmospheric Transmissivity 50.3 GHz

VII. Simulated Visibilities

Currently, the algorithm for conversion of T_B images to visibilities utilizes the 2D FFT in rectangular coordinates for speed and simplicity. The differences in the output between the rectangular and hexagonal sampling are not significant for determining the magnitude of the spatial power spectral density. A hexagonal sampling version is pending. Antenna patterns and tapers can be applied in the visibility domain to evaluate their effects. The G-Matrix formulation is currently avoided as it is too computationally expensive for this trade-off analysis.

Figure 4 is a scatterplot of the visibility function generated from the T_B image shown in Figure 1 as a function of antenna-pair baseline in units of wavelengths. Note: Both axes are plotted on log scales. The vertical line shows approximately the extent of visibilities that the 50 GHz channels of GeoSTAR will be able to measure with 100 antennas per arm extending 2.25 m. This effectively shows the components of high spatial

frequency that GeoSTAR fails to measure which leads to the Gibbs phenomenon in the reconstructed image.

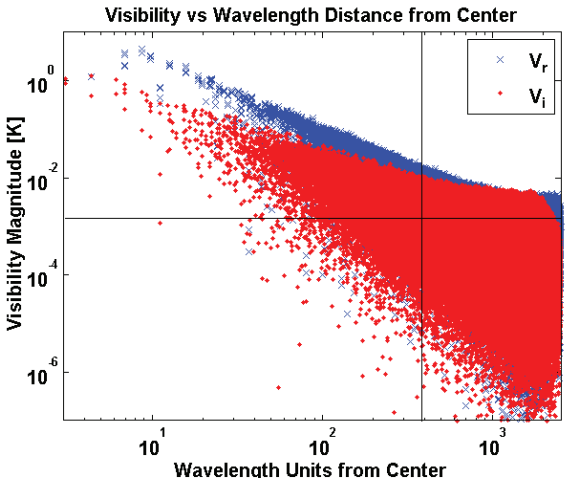

Figure 4: Simulated Visibilities vs. Wavelength Distance from Center

The antenna pattern applied is typical of the parabolic Potter horn as described in [1]. This typical distribution of visibilities demonstrates that the variation in magnitude increases away from the center, and the maximum magnitude decreases as expected. The horizontal line in Figure 4 assumes an NEΔV of 1.5 mK which is obtained with ~15 minutes of integration, a single measurement channel and T_{sys} of ~400K. This NEΔV value results in a 1 K pixel error in the image. At this level, the additive noise has the same power level as many of the high frequency visibilities. With these signal to noise ratios, it will be difficult to discern visibility variability from measurement noise, especially for the larger baselines.

VIII. Conclusions

A high resolution full disk model has been created that generates top of atmosphere 50 GHz T_B images as seen from a GOES location. The model utilizes existing datasets to provide realistic inputs of the atmospheric state and can be generated with varying initialization states (no winds, no clouds, etc) that provide insight into that particular parameter's contribution to the T_B images. Images can generated for various frequencies of measurement allowing for the evaluation of atmospheric profile retrievals. Visibilities are generated using an ideal 2D FFT in rectangular coordinates to determine the expected distribution in the visibility domain.

High resolution visibility maps allow for the evaluation of various instrument design parameters. Different antenna designs can be implemented easily to determine their impact on the visibilities. Reducing the reconstructed image spatial resolution can be modeled by truncating the high frequency visibilities above the instrument resolution level. This process is equivalent to sub-sampling the original image. The model already yields valuable results in the form of the actual visibility magnitudes to be expected for a typical measurement. The impact of changing various instrument parameters can be evaluated with respect to the final measurement using actual scenes.

IX. Acknowledgements

The authors would like to thank all the dataset providers, in particular, the NASA Langley Cloud and Radiation Research Group for use of their full disk cloud product and Dr Fatima Karbou for the AMSU land emissivity atlases. This work was supported by NASA Headquarters under the NASA Earth and Space Science Fellowship Program – Grant NNG05GP47H.

X. References

[1] A. B. Tanner, W. J. Wilson, B. H. Lambrigsten, S. J. Dinardo, S. T. Brown, P. P. Kangaslahti, T. C. Gaier, C. S. Ruf, S. M. Gross, B. H. Lim, S. Musko, S. Rogacki, and J. R. Piepmeier, "Initial Results of the Geostationary Synthetic Thinned Array Radiometer (GeoSTAR) Demonstrator Instrument," *Geoscience and Remote Sensing, IEEE Transactions on*, vol. 45, pp. 1947, 2007.

[2] B. Lambrigtsen, W. Wilson, A. Tanner, T. Gaier, C. Ruf, and J. Piepmeier, "GeoSTAR - a microwave sounder for geostationary satellites," presented at Geoscience and Remote Sensing Symposium, 2004. IGARSS '04. Proceedings. 2004 IEEE International, 2004.

[3] A. B. Tanner, B. H. Lambrigsten, and T. C. Gaier, "A dual-gain antenna option for GeoSTAR," presented at Geoscience and Remote Sensing Symposium, 2007. IGARSS 2007. IEEE International, 2007.

[4] F. Torres, A. B. Tanner, S. T. Brown, and B. H. Lambrigsten, "Analysis of Array Distortion in a Microwave Interferometric Radiometer: Application to the GeoSTAR Project," *Geoscience and Remote Sensing, IEEE Transactions on*, vol. 45, pp. 1958, 2007.

[5] D. H. Staelin and C. Surussavadee, "Precipitation Retrieval Accuracies for Geo-Microwave Sounders," *Geoscience and Remote Sensing, IEEE Transactions on*, vol. 45, pp. 3150, 2007.

[6] P. Rabindra, P. Minnis, D. A. Spangenberg, M. M. Khaiyer, M. L. Nordeen, J. K. Ayers, L. Nguyen, Y. Yi, P. K. Chan, Q. Z. Trepte, F. L. Chang, and W. L. Smith, Jr., "NASA-Langley web-based operational real-time cloud retrieval products from geostationary satellites," 2006.

[7] L. Klein and C. Swift, "An improved model for the dielectric constant of sea water at microwave frequencies," *Antennas and Propagation, IEEE Transactions on [legacy, pre - 1988]*, vol. 25, pp. 104, 1977.

[8] G. Deblonde and S. English, "Evaluation of the FASTEM2 Fast Microwave Oceanic Surface Emissivity Model," presented at International ATOVS Study Conference, Budapest, Hungary, 2000.

[9] P. Rosenkranz, "Water vapor microwave continuum absorption: A comparison of measurements and models," *Radio Sci.*, vol. 33, pp. 919-928, 1998.

[10] D. Staelin, "Measurements and Interpretation of the Microwave Spectrum of the Terrestrial Atmosphere near 1-Centimeter Wavelength," *J. Geophys. Res.*, vol. 71, pp. 2875-2881, 1966.

[11] E. M. Feæigel§son, *Light and heat radiation in stratus clouds: (Radiatsionnye protsessy v sloistoobraznykh oblakakh*. Jerusalem: Israel Program for Scientific Translations; [available from the U.S. Dept. of Commerce, Clearinghouse for Federal Scientific, and Technical Information, Springfield, Va.], 1966.